2020

An ab initio study on the effects of Na passivation on friction reduction of an iron oxide surface

Nam Van Tran
University of Wollongong, vnt981@uowmail.edu.au

Anh Kiet Tieu
University of Wollongong, ktieu@uow.edu.au

Hongtao Zhu
University of Wollongong, hongtao@uow.edu.au

Thi Thuy Huong Ta
University of Wollongong, ttht664@uowmail.edu.au

Manh Ha Le
University of Wollongong, mhl980@uowmail.edu.au

See next page for additional authors

An ab initio study on the effects of Na passivation on friction reduction of an iron oxide surface

Abstract

The presence of sodium-rich layers on iron oxide surfaces plays an important role in the functionality of glassy lubricants used in harsh working conditions of metal formation. However, the underlying low-friction mechanism of the sodium layer on iron oxide surfaces at the atomic level is not well understood. In this work, Na adsorption on the most stable surface of Fe_2O_3 (0001) is studied by density functional theory. The most stable adsorption configuration and the modifications induced by the adsorption on the structural as well as the electronic properties of the surface are discussed. By constructing the potential energy surface, we can quantitatively compare the sliding behaviors of two sodium passivated oxide layers with that of clean surfaces. The determination of energy corrugations, sliding paths, static lateral forces, and shear strengths has suggested a significantly lower friction in the Na-passivated system compared to that of the clean surface. The effects of a load on the friction are also investigated. The results indicate that sodium passivation in glass lubricants can help to prevent the direct contact of two oxide surfaces and thereby maintain a low friction and hence wear reduction at high pressures.

Disciplines

Engineering | Science and Technology Studies

Publication Details

Tran, N. V., Tieu, A. K., Zhu, H., Ta, H. T. T., Le, H. M. & Ta, T. D. (2020). An ab initio study on the effects of Na passivation on friction reduction of an iron oxide surface. Journal of Applied Physics, 127 (6), 065305-1-065305-13.

Authors

Nam Van Tran, Anh Kiet Tieu, Hongtao Zhu, Thi Thuy Huong Ta, Manh Ha Le, and Thi D. Ta

Journal of Applied Physics ARTICLE scitation.org/journal/jap

An *ab initio* study on the effects of Na passivation on friction reduction of an iron oxide surface

Cite as: J. Appl. Phys. **127**, 065305 (2020); doi: 10.1063/1.5133078
Submitted: 23 October 2019 · Accepted: 18 January 2020 ·
Published Online: 11 February 2020

Nam V. Tran, Anh K. Tieu,[a] Hongtao Zhu,[a] Huong T. T. Ta, Ha M. Le, and Thi D. Ta

AFFILIATIONS

School of Mechanical, Materials, Mechatronic and Biomedical Engineering, Faculty of Engineering and Information Sciences (EIS), University of Wollongong, Northfields Avenue, Wollongong, NSW 2522, Australia

[a]**Authors to whom correspondence should be addressed:** ktieu@uow.edu.au and hongtao@uow.edu.au

ABSTRACT

The presence of sodium-rich layers on iron oxide surfaces plays an important role in the functionality of glassy lubricants used in harsh working conditions of metal formation. However, the underlying low-friction mechanism of the sodium layer on iron oxide surfaces at the atomic level is not well understood. In this work, Na adsorption on the most stable surface of Fe_2O_3 (0001) is studied by density functional theory. The most stable adsorption configuration and the modifications induced by the adsorption on the structural as well as the electronic properties of the surface are discussed. By constructing the potential energy surface, we can quantitatively compare the sliding behaviors of two sodium passivated oxide layers with that of clean surfaces. The determination of energy corrugations, sliding paths, static lateral forces, and shear strengths has suggested a significantly lower friction in the Na-passivated system compared to that of the clean surface. The effects of a load on the friction are also investigated. The results indicate that sodium passivation in glass lubricants can help to prevent the direct contact of two oxide surfaces and thereby maintain a low friction and hence wear reduction at high pressures.

I. INTRODUCTION

The application of inorganic glasses as a lubricant in harsh working conditions has received tremendous attention in recent years because of their good lubricating performance, low cost, and environmentally friendly properties.[1] Particularly, the most recent tribological tests have demonstrated the efficiency of sodium silicate, borate, and phosphate glasses in terms of friction reduction, antiwear, and antioxidation with an operating temperature up to 900 °C.[2–4] The properties of a complex glass system can change significantly by controlling the type as well as the concentration of the cation elements.[5–10] The concentration of these cation elements has a great effect on the mobility-related properties of glasses such as ionic diffusion, electrical conductivity, chemical durability, dielectric relaxation, internal friction, and viscosity.[11–15] Consequently, the tribological properties of glass lubricants can be effectively modified by changing the alkali metal and its concentration. Although an extensive amount of information has been drawn to explain the tribofilm formation as well as the tribochemistry of glassy lubricants, the lack of atomic and electronic insights in the present experimental studies still challenges scientists to fully understand the true mechanism of the lubricants.

Experimental studies have shown that alkali elements play an important role in tribological performance for glass lubricants under extremely high pressures and elevated temperatures in metal forming processes. The formation of the Na-rich layer in the tribofilm is believed to deliver a great contribution to the friction-reduction as well as wear-protection properties[16–18] of steel-on-steel sliding contacts, i.e., the presence of sodium cations in the borate lubricant leads to a significant improvement of lubricity compared to the sole boron oxide.[19] A similar observation has been reported by Wan *et al.*[17,20] using a sodium phosphate glass lubricant. A recent experiment on the effect of melted sodium metasilicate on mild steel revealed that the produced tribofilm is mainly composed of sodium from the glass and manganese diffusing from the steel surface.[21] Although experimental studies have provided much evidence about the significance of alkali elements in the role of friction reduction, a clear understanding of the observation is still not available. There are still a number of open questions to be unveiled, such as: What is the mechanism that drives the low friction and wear of the sodium-rich layer tribofilm? Can sodium alone provide a good lubricating performance? Or what are its effects on the anti-oxidation properties of the steel surface?, and more. In order to

provide a physical explanation for these experimental observations, it is crucial to understand the effect of sodium on frictional properties and its mechanism at the atomic level.

In the last few years, there has been a limited number of experimental and theoretical works on the influence of alkali metal doping on different surfaces of iron oxide,[22] but no detailed investigation on the adsorption of alkali elements on the Fe_2O_3 (0001) surface has been published. Currently, it is still unclear how sodium adsorption may alter the structural and electronic properties of the iron oxide surface and to what degree this phenomenon is related to the reduction of friction and wear. While the conventional method for simulating the nanoscale friction is classical molecular dynamics (MD), a clear drawback is the lack of ability to simulate the electronic properties such as electron transfer, Pauli repulsion, mutual polarization, electron exchange, and correlation that could limit its applications.[23] In addition, the parameters of these classical MD potentials are optimized to reproduce only certain properties of the modeled systems. Therefore, the potentials may fail to provide the correct results if the investigated systems or properties change.[23] On the other hand, *ab initio* approaches have become the more common tool to investigate the tribological properties of materials in recent years,[16,24–31] thanks to the advantages in providing a high accuracy and insight into the atomic origin of tribochemical reactions. At the same time, the increasing power of computers keeps the simulation time manageable. One effective practice to investigate friction at an atomic scale is to perform potential energy surface (PES) calculations.[27,28,32] This simulation procedure has been successfully applied to predict frictional properties for a wide range of systems from 2D materials such as graphene[33] to passivated surfaces like Fe (110) adsorbed by sulfur.[32]

In this work, a systematic theoretical study based on Density Functional Theory (DFT) of frictional behaviors of the Na passivated Fe_2O_3 (0001) surface is reported. The idea was inspired by the experimental results indicating that sodium in the molten glass is attracted by the oxide surface.[18,19,21] As a result, sodium is drained from the glass lubricant and absorbs on the surface creating a sodium-rich film that covers the outermost layer of the steel substrate. Therefore, the current study only focuses on the effect of the sodium-rich layer on friction reduction. However, there are other elements of the glass that involve and affect the properties of the Na-rich layer. They not only influence the formation of the sodium layer but can also react and cause the structural modification of the metal oxide surface. To tackle the roles of these elements, a different methodology allowing to simulate a whole glass structure interacting with the metal oxide surface at high temperatures is necessary. Therefore, the roles of these elements will be discussed in a separate work. Nonetheless, the currently obtained results on Na have improved our understanding of its role within the glass lubricant and provided helpful data for the design and development of alkali glass-based lubricants.

It is well-known that hematite and magnetite are the most stable phases among all the polymorphs of iron oxides at elevated temperatures. However, in the condition of rich oxygen and high pressure, hematite is more stable compared to magnetite. Ketteler *et al.* calculated free energies for several iron oxide phases at the temperature of 1000 K for different oxygen partial pressures.[34] Their result indicated that the free energies are similar at low pressures, suggesting that all phases may coexist. However, when pressure increases, hematite becomes more stable compared to other phases. In this study, we clarify the most stable adsorption configuration of sodium on the surface and calculate the adsorption-induced modifications in the electronic structure of the surface. The comparison of the potential energy surface of pure and Na adsorbed Fe_2O_3 (0001) surfaces allows us to identify the most notable trend and the impact of the metal passivation on the friction reduction. Particularly, we found that the adsorption of Na on the iron oxide surface can cause a depletion of charge density difference at the sliding contact. As a consequence, it leads to a collapse of PES and reduces friction. In addition, the sodium passivated surface has a specific mechanism to minimize the charge redistribution at the interface by dispersing the charge transfer out of the interface.

II. COMPUTATIONAL DETAILS

DFT simulations were performed using the Quantum Espresso package[35,36] to optimize and calculate the energy as well as electronic structures of various iron oxide systems. The electron exchange and correlation effects were calculated using the generalized gradient approximation (GGA) of Perdew–Burke–Ernzerhof exchange and correlation functional.[37,38] The ultrasoft pseudopotentials method was used to represent the interactions between valence electrons and ionic cores,[39] and the electronic wave functions were expanded in a plane-wave basis with a kinetic energy cut-off energy of 50 Ry for wavefunctions and 400 Ry for charge density. The k-point mesh was constructed using the Monkhorst–Pack (MP) algorithm[40] and a Gaussian broadening with a smearing width of 0.01 Ry. A k-point mesh of $3 \times 3 \times 1$ was used for the integration of the Brillouin during ionic optimizations, while a denser grid of $5 \times 5 \times 1$ was applied for electronic structure calculations. The convergence criteria of 10^{-6} Ry for the electronic self-consistent loop and 10^{-5} Ry for ionic relaxation were applied for all calculations. Previous studies have shown that including van der Waals correction will yield more accurate results in the electronic structures, ground-state properties of metallic surfaces,[41] and transition metal oxides.[42] Therefore, a semiempirical van der Waals correction obtained by Grimme[43,44] was also included in all of our simulations.

As a prototype system to study the nanoscale frictional model, we considered two slabs of Fe_2O_3 (0001) in a dry contact. The selected direction is based on previous publications which indicate that the Fe_2O_3 (0001) surface with Fe–O_3–Fe termination is the most thermodynamically stable surface morphology of Fe_2O_3.[45,46] The slabs were modeled by a periodic supercell of a 2×2 in-plane size as shown in Fig. 1. Each slab contains nine atomic layers, which is thick enough to obtain accurate electronic properties while retaining computational efficiency.[47] A vacuum region of 15 Å has been added along the z-direction to prevent the interaction between the periodic images. The ionic positions of each slab are prerelaxed for further calculations, except for those belonging to the three bottom layers of both the slabs.

PES caused by the displacement of the upper slab above the lower one was generated using a scanning process. A mesh grid of different relative lateral positions of the two slabs was used to determine the system energy.[48] Particularly, we examined 49 symmetry positions (the 7×7 grid is shown in Fig. 1) which can be obtained

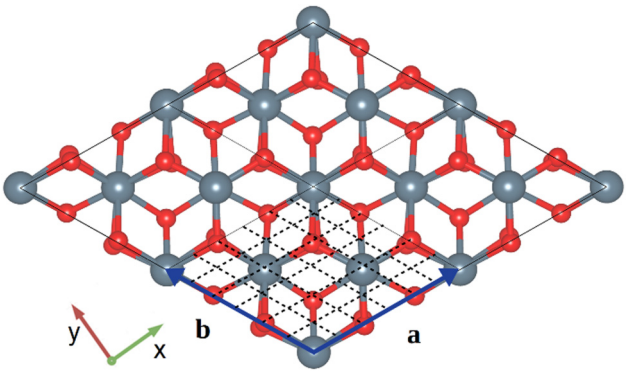

FIG. 1. Top view of the optimized structure of the Fe_2O_3 (0001) surface. Only the three topmost atomic layers are shown. Grey and red balls represent iron and oxygen atoms, respectively. The grid used to calculate the PES of two oxide slabs in relative motion is represented by the dashed lines. Each grid point represents the position of the iron atom belonging to the 2 × 2 supercell of the upper surface (not shown) within the supercell of the lower slab.

by shifting the upper slab along **a** and **b** directions to create sample points for the calculation of system energy. The atoms of the top slab were relaxed in the z-direction every time the slab moves to a new position, while the x and y coordinates were fixed during the scanning process.[25,49,50] Meanwhile, the atoms of the three bottom layers of the lower slab were fixed at the bulk structure. PES was then derived from the system energy using the lowest system energy as the reference (that corresponds to the shift in the lowest energy of the PES to zero),

$$E_{sys} = (E_{tot} - E_{tot-min})/N, \tag{1}$$

where E_{tot} is the total energy of the simulation system with two slabs in contact with each other, $E_{tot-min}$ represents the lowest energy of the system,[49] and N is the total number of atoms in the supercell. The cubic spline interpolation was then applied to refine this grid (generate more grid points) and created a smooth PES. Another important quality in tribological modeling is the binding energy of two layers which is defined as

$$E_{bind} = (E_{tot} - 2E_{single})/N, \tag{2}$$

where E_{single} is the energy of a separated layer. The binding energy is used to evaluate the work required to separate a single layer from a substrate,[32,49,51] thus providing the essential information to understand the binding strength between the two surfaces.

In order to investigate the influence of sodium passivation on friction, PES and binding energy of Fe_2O_3 slabs with Na passivated were also calculated. First, we have calculated the adsorption energy for different adsorption sites of sodium on the iron oxide surface. The detail of the adsorption sites is discussed in the supplementary material. The adsorption energy was calculated by subtracting the total energy of the interaction system to the energy of the separated surface and sodium atoms. We then normalized the adsorption energy by the total number of adatoms in the system,[52]

$$E_{ad} = (E_{tot} - E_{surf} - nE_{adatom})/n, \tag{3}$$

where E_{surf} is the energy of the iron oxide surface, n and E_{adatom} are the number of sodium atoms and its energy, respectively. In order to compare with the shearing of the pure Fe_2O_3 surface, the PES of the Na passivated surface was also calculated using the most stable adsorption configuration of sodium. The process is similar to that for the pure Fe_2O_3 slab as mentioned previously.

III. RESULTS AND DISCUSSIONS

A. Adsorption of sodium on the Fe_2O_3 (0001) surface

To find the most stable adsorption position of sodium on the iron oxide surface, we consider a supercell of (2 × 2). The adatom is placed on five different high-symmetry sites (see Fig. S1 in the supplementary material), a structure relaxation is then performed on these initial configurations. The energy comparison indicates that the sodium atom prefers to adsorb on the hollow position (HL) of the Fe_2O_3 (0001) surface, where it can bind to three oxygen atoms of the substrate (Table S1 in the supplementary material). The hollow position allows the sodium atom to obtain the highest coordination number with the oxygen atoms compared to other different adsorption sites. The adsorption distance between sodium and the oxygen atom of the surface is 2.3–2.4 Å (Na–Na distance is 2.9 Å). This distance is similar to a typical O—Na bonding distance in sodium silicate or phosphate glass.[53,54] We are not aware of any previous work about the adsorption of sodium on the Fe_2O_3 (0001) surface.

There are two hollow positions (HLs) per unit cell of the Fe_2O_3 (0001) surface. Therefore, two difference adsorption coverages (half coverage and full coverage) have been considered (Fig. 2). The calculation of the adsorption energy at different coverages of sodium is shown in Table S2 in the supplementary material. The result indicates that a lower concentration of sodium on the surface results in a slightly larger adsorption energy than that with a higher Na concentration. Nonetheless, the adsorption is stable for both low and high coverages, which is indicated by high absorption energies (Table S2 in the supplementary material). In fact, the calculated adsorption energy is much higher than those of several metal atoms such as Au (1.53 eV) and Pd (1.82 eV) adsorbed on the iron oxide surface.[55] It is also worth mentioning that, in the ambient condition such as room temperature and high humidity, the hematite (0001) surface will be expected to be hydroxylated. However, at the working condition of glassy lubricants or hot metal formation, the temperature can reach 1173 K or above, the surface can be dehydroxylated and excessive water will be evaporated.[56] In fact, a thermal decomposition has been used for a long time to treat the surface of a metal oxide such as iron oxide[57–59] or aluminum oxide.[60] Therefore, the hydroxylated hematite (0001) surface is not considered in the present report.

B. Frictional behaviors of iron oxide surface

Before investigating the effect of sodium passivation on the friction of the iron oxide surface, the PES, binding energy,

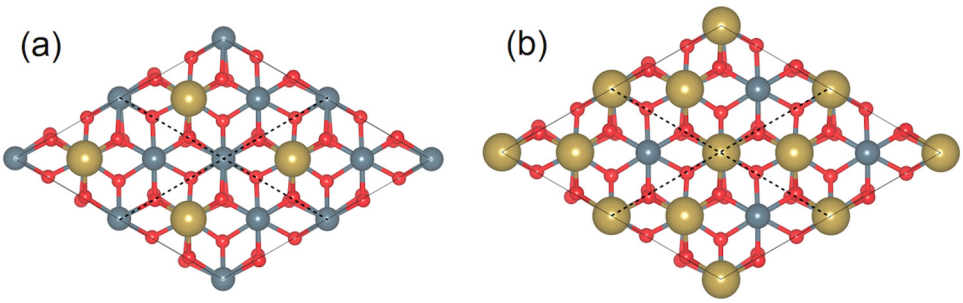

FIG. 2. The adsorption configuration sodium on the Fe_2O_3 (0001) surface is reported in a top-view representation. (a) One sodium atom per unit cell (half coverage). (b) Two sodium atoms per unit cell (full coverage). Sodium atoms are illustrated by yellow balls, iron and oxygen are in the same colors as those in Fig. 1. The dashed line represents the unit cells of the surface.

corrugation energy, as well as the electronic structure of two sliding pure iron oxide surfaces were first calculated to create a reference. The information is also very useful since it provides us with knowledge about the factors that lead to the high friction of the iron oxide surface. As a consequence, these factors can provide us with options to control the friction of the oxide surface.

Figure 3(a) shows the PES plot of the Fe_2O_3 system. The maximum and minimum energy values are marked, and their corresponding configurations are shown in Figs. 3(b) and 3(c). In general, the PES indicates that the sliding energy profiles of the iron oxide surfaces can be characterized by two different minima (labeled as Min1 and Min2) with relatively similar energies and a maximum (labeled as Max). The PES reaches its maximum energy at 46.5 meV/atom, when the iron atoms on the upper slab are on the top of the Fe atoms of the bottom slab [Fig. 3(b)]. Meanwhile, at the minimum energy of the PES, the iron atoms are located just above the center of the triangle which is formed by the three adjacent O atoms of the lower slab [Fig. 3(c)]. When sliding from the maximum to the minimum energy configuration, the binding energy of the two layers increases from 72.7 meV/atom to 119.2 meV/atom (Table I). The increasing binding energy is related to the strong interaction of the two layers at the minimum energy configurations. For this stacking, the Fe atoms are allowed to form multiple Fe—O bonds between the two layers. Because of the strong interaction between the upper iron atoms and lower oxygen atoms, the interlayer distance d in the minimum energy configuration (1.27 Å) is much smaller than that of the maximum one (1.88 Å). The decline of the interlayer distance at the minimum energy configuration could give rise for strong Fe—O covalent bonds between the two layers. The calculated Fe—O bond length between two layers indicates that the Fe—O bond length is 1.89 Å, which is slightly smaller than that of the bulk system (1.97 Å). Therefore, the high binding energy of the two Fe_2O_3 layers at the stable stacking could be due to the formation of the Fe—O covalent

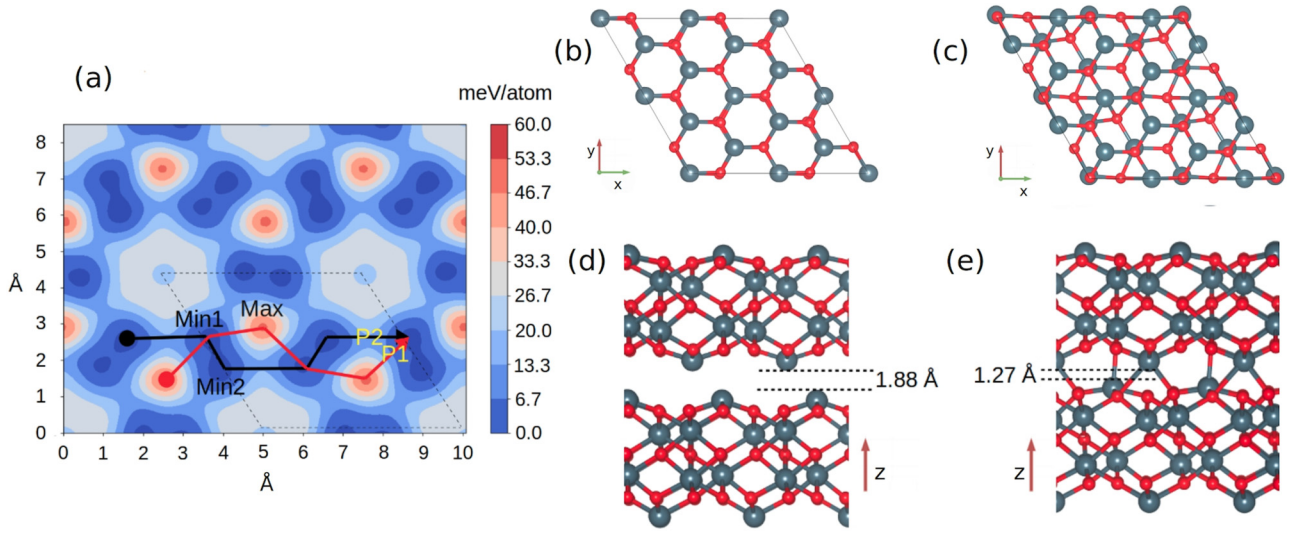

FIG. 3. PES as a function of relative displacement of the two oxide layers in the x and y directions (a), the black and red solid line mark the minimum and maximum energy pathways, the dashed line represents a unit cell. Geometric arrangement for the most important stacking configurations [maximum (b) and minimum (c) energy] in the PES of clean oxide surfaces, the bottom pictures (d) and (e) show a side view of the corresponding structure, respectively. Only the three topmost atomic layers of the lower slab and three bottom layers of the upper slab are shown in the top view images.

TABLE I. Comparison of system energy corrugation ΔE (E_{max}–E_{min}), averaged static lateral force $|F|$, shear strength τ, binding energy $|E_{bind}|$, and charge redistribution ρ_{redist} for the clean and sodium passivated iron oxide surfaces. The notation in the bracket indicates the sliding pathway or the stacking configuration. P1 and P2 indicate the maximum and minimum energy pathways respectively. Max and Min denote the maximum and minimum energy stacking configurations as shown in Figs. 3(a) and 7(a).

Systems	$\lvert F\rvert$ (meV/Å atom)	τ ($\times 10^{-3}$ GPa/atom)	ρ_{redist} ($\times 10^{-4}$ e/Å^3)	$\lvert E_{bind}\rvert$ (meV/atom)	ΔE (meV/atom)
Fe_2O_3	27.4 (P1)	50.0 (P1)	40.0 (Min2)	119.2 (Min2)	46.5
	17.0 (P2)	31.0 (P2)	22.9 (Max)	72.7 (Max)	
Na-Fe_2O_3	4.3 (P1)	7.9 (P1)	14.6 (Min)	65.1 (Min)	12.5
	1.7 (P2)	3.1 (P2)	20.0 (Max)	52.6 (Max)	

bonds which, in turn, suggests a high sliding resistance in this system.

The mutual interaction between two surfaces will lead to a redistribution of electronic charge at their interface. These charge redistributions allow us to understand the fundamental mechanism of adhesion or friction at the microscopic scale.[61–63] It has been proven that the charge redistribution at the stable stacking configuration of two sliding surfaces has a linear relationship with their friction.[32] The charge density difference is obtained by subtracting the electronic charge of the interface to that of the two separated surfaces, $\Delta\rho(r) = \rho_{sys}(r) - (\rho_{top}(r) + \rho_{bot}(r))$. As shown in Fig. 4, the main source of the charge reconstruction comes from the electron depletion and accumulation between the top layer Fe atoms and O atoms of the bottom layer and vice versa. The terminated oxygen and iron atoms on the surface are, therefore, more chemically active due to its ability to donate and receive electrons respectively. The calculated PDOS in Fig. 5 shows that the O 2p states of the bottom layer strongly overlap with the Fe 3d states of the top layers. By contrast, the maximum stacking configuration shows a much smaller charge redistribution. To quantify this charge density redistribution, we integrate the absolute value of the planner average ρ_{diff} [Fig. 4(b)] of the charge density difference at the interface region,[32]

$$\rho_{redist} = \frac{1}{d}\int_{z_1}^{z_2} |\rho_{diff}|dz. \tag{4}$$

The data in Table I indicate that the charge redistribution of the minimum configuration is quite high, i.e., almost double that of the maximum configuration. The result is consistent with the calculated bond lengths as well as the binding energy of the two Fe_2O_3 surfaces, which indicates the strong Fe–O covalent bonds between the two slabs.

The most energetically favorable and unfavourable sliding pathways are presented in Figs. 3(a) and 6. The barrier energy for sliding along the minimum energy pathway (P1) is 22.4 meV/atom, which is less than half of that length of the maximum one (P2, 46.5 meV/atom). The averaged lateral force F experienced by the upper slab during the sliding along the two pathways (P1 or P2) is calculated using the method proposed by Zhong and Tománek,[64]

$$F = |\Delta E_b|/\Delta r, \tag{5}$$

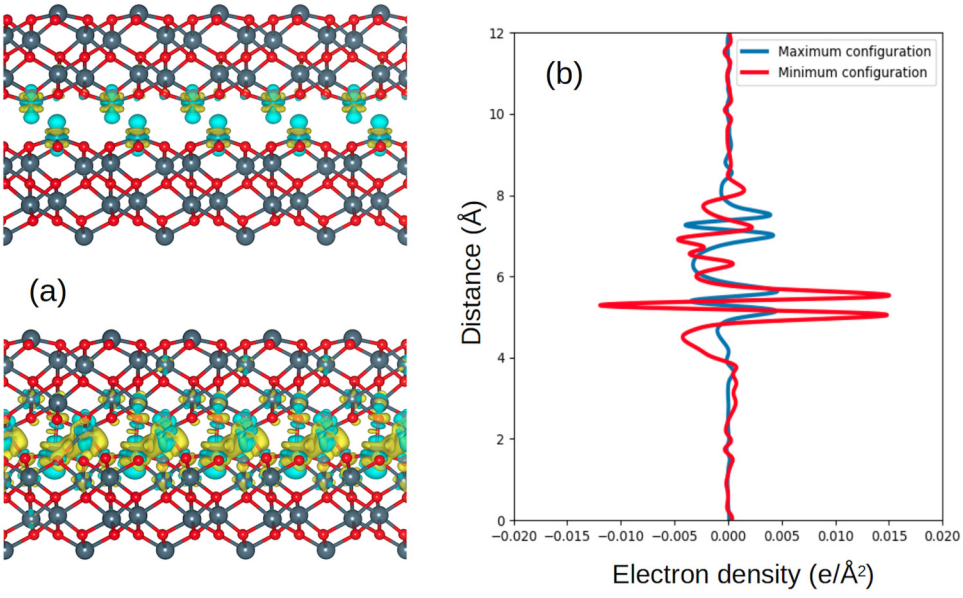

FIG. 4. (a) Charge density difference for the least (top) and most (bottom) stable stacking configurations of the two clean surfaces in contact. The yellow and cyan represent the positive (electron accumulation) and negative (electron depletion) regions, respectively (isosurfaces are 0.005 e/Å^3). (b) Planar average of the electronic charge displacements occurring upon the stacking of two iron oxide surfaces. Blue and red colors are used for the charge displacements calculated respectively for the least and most favorable lateral positions.

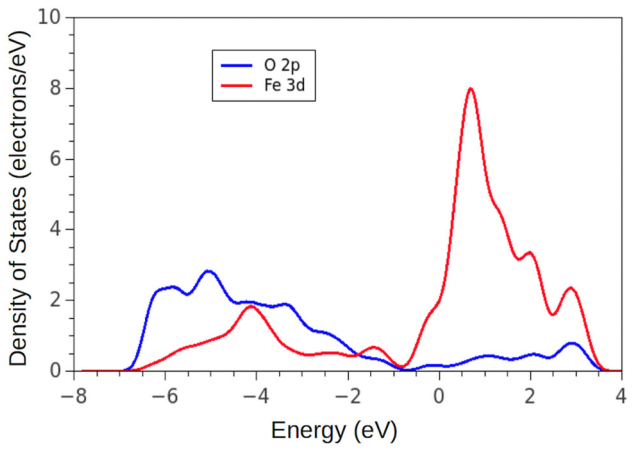

FIG. 5. PDOS for oxygen and iron atom at the interface of the minimum energy configuration of two pure Fe_2O_3 (0001) surfaces.

where ΔE_b and Δr are the barrier energy and the sliding displacement along the maximum and minimum energy pathways, respectively. The calculated averaged lateral force in Table I shows that the sliding along pathway P1 has a lateral force of 17.0 meV/Å per atom, which is 10.4 meV/Å per atom lower than along the maximum energy pathway (P2), indicating that the friction could rise more than 37.5% along path P2. Another important merit that is often used by scientists to quantify the friction of two sliding surfaces is the corrugation energy ΔE. The quality is measured by the difference between the maximum and minimum of the PES, which is equal to the highest peak of the PES in our case since we have shifted the minimum value to zero. This value is crucial since it estimates the maximum amount of energy per atom that might be dissipated by

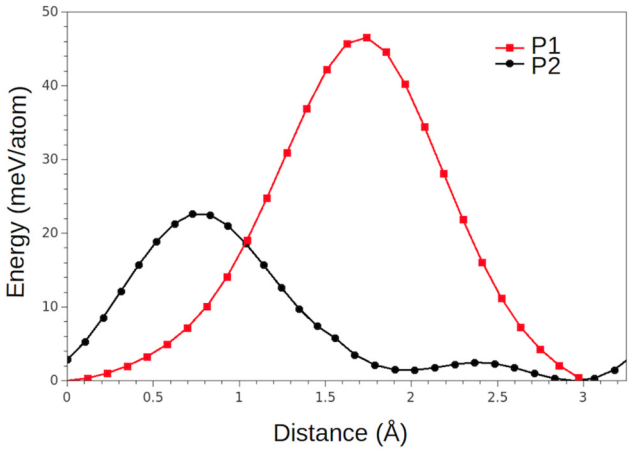

FIG. 6. Variation of the system energies with the sliding displacement along the maximum (red line) and minimum (black line) energy pathways marked in Fig. 3(a).

frictional processes. It has been proven that reducing the corrugation energy ΔE by surface passivation using lubricant additives could lead to the reduction of friction in several systems.[65] The calculated corrugation energy (46.5 meV/atom) of two sliding Fe_2O_3 slabs (Table I) is very high, making it hard to switch from a stable position to an unstable position which suggests a high friction. For the purpose of comparison, the corrugation energy of graphene, which provides superlubricity, is approximately 1.41 meV/atom.[49] Therefore, a surface treatment is necessary in this case to reduce friction. In Sec. III C, we will examine the effect of sodium passivation on the tribological properties of the iron oxide surface.

C. Effects of sodium passivation on tribological properties

The chemical and physical behaviors of the iron oxide surface at an atomic scale can be modified by the passivation of alkali atoms. Similar to the macroscopic roughness, the surface modification can greatly influence the frictional properties of the system. In order to understand the influence of sodium passivation on the frictional properties, we examine the change in the morphology of PES.

According to previous experimental studies of sodium glass lubricants at high temperatures and pressures, the tribofilm shows a thick layer of sodium on top of the iron oxide layer.[17,18] The results suggested that sodium adsorbs on the oxide surface at a high concentration and prevent direct contact between two sliding oxide surfaces. Therefore, in this study, we cover all of the favorable hollow positions on the Fe_2O_3 surface by the sodium atoms (full coverage) as shown in Fig. 2(b). Furthermore, our testing potential energy surface at low coverage adsorption (one adatom per unit cell) does not show a reduction of friction. In fact, at low coverages, the PES calculation shows a higher friction compared with that of the clean iron oxide surface. It is worth mentioning that, the corrugation energy is not reduced even though the number of Fe–O bonds is still mitigated in the case of low coverage absorption. There are possibly two reasons for the phenomena. First, at the minimum energy configuration of the lower coverage system, the sodium atoms of the bottom and the top surfaces arrange into a single layer [Fig. S3(b) in the supplementary material]. We believe that this layer could stick the two surfaces through electrostatic interaction and increase the corrugation energy, which is opposite to the case of the full coverage, where two separate layers of Na are formed and interact through repulsive forces. Second, together with the alignment of the sodium layer at the low coverage, the Fe atoms of the bottom slab are relaxed inward into the bulk structure [Fig. S3(b) in the supplementary material]. This modification leaves the surface with an oxygen layer on top, thus promotes electrostatic attraction among Fe_2O_3—Na—Fe_2O_3 stacking, and consequently leads to the stable stacking of the two surfaces as well as the high corrugation energy. The result suggests that the iron oxide surface needs to be covered by a high concentration of sodium in order to reduce the friction. Hence, in this section, we only focus on the high coverage adsorption of sodium atoms. The calculation for the adsorption energy at different coverages as well as PES can be found in the supplementary material.

The contour plot of the PES for the Na passivated Fe_2O_3 (0001) surface is shown in Fig. 7(a). A similar color representation

scale with the case of pure iron oxide surface is used for the purpose of comparison. By comparing with Fig. 3(a), the shape of PES undergoes a significant change when the surface is passivated by sodium atoms. It can be found that the sliding energy profile of the Na-passivated Fe_2O_2 layer is characterized by only one minimum (labeled as Min) and a maximum (labeled as Max) compared to two minima in the case of the pure iron oxide surface. The highest energy stacking configuration of pure iron oxide surfaces now turns into the lowest energy configuration as shown in Fig. 7(a). Meanwhile, the maximum energy stacking occurs when the sodium atoms of the upper slab are just above the sodium atom on the lower slab [see Fig. 7(b)]. Furthermore, the PES becomes much flatter compared with that of the pure surface, indicating a significant reduction of the energy corrugation [Fig. 7(a)]. It is predicable that the energy required to break Fe–O interlayer covalent bonds between clean oxide surfaces is much higher than that for the Na–Na electrostatic interactions when the substrates are passivated. The calculated binding energy (Table I) at the stable stacking configuration is 65.1 meV/atom, which is almost half of the value obtained from the pure oxide surfaces (119.2 meV/atom). It is worth mentioning that the smooth PES indicates the vanishing of energy dissipation by phonons.[28] Since the higher is the energy dissipation, the stronger the adhesive bonding between two sliding surfaces, the minimization of the energy dissipation will reduce friction.[66,67] Although there are other mechanisms, a number of publications have pointed out that the phonon dissipation can play an important role in the dissipating energy process.[62,68,69]

The interlayer distance also experiences a significant change when the surface is passivated by sodium atoms. The result mainly comes from the columbic force between the upper sodium atoms with the lower one. The adsorption of sodium on the Fe_2O_3 surface replaces the strong Fe–O covalent bonds by weak electrostatic interaction between the two sodium layers. Since sodium or alkali atoms, in general, are positively charged, the repulsive interactions between them will force the two surfaces to move further leading to a wide gap between them. As a consequence, the adsorption of sodium can reduce direct surface–surface contact when sliding. In addition, the weaker electrostatic interaction compared with the covalent bond allows the two surfaces to adjust their interlayer distance more flexibly. As shown in Figs. 7(d) and 7(e), the interlayer distances at the maxima (3.23 Å) and the minima (2.22 Å) of the passivated iron oxide surfaces are ~1.7 times longer than those of the clean Fe_2O_3. Therefore, the reduction of interlayer distance when sliding from the maximum to the minimum energy configurations is also more significant in this case. As the interlayer distance is always kept at a high value, the adsorption of sodium not only lowers friction but also reduces wear by preventing the direct contact between the two sliding steel surfaces.

The variation of the charge density redistribution during the sliding of the top layer is shown in Figs. 8(a) and 8(b), which indicates that they are strongly affected by the adsorption of sodium atoms on the surface. For instance, when sliding from the maximum to the minimum energy configurations, the sodium passivated surface shows a significant reduction in the charge distribution compared to that of the clean surface [Figs. 4(a) and 4(b)].

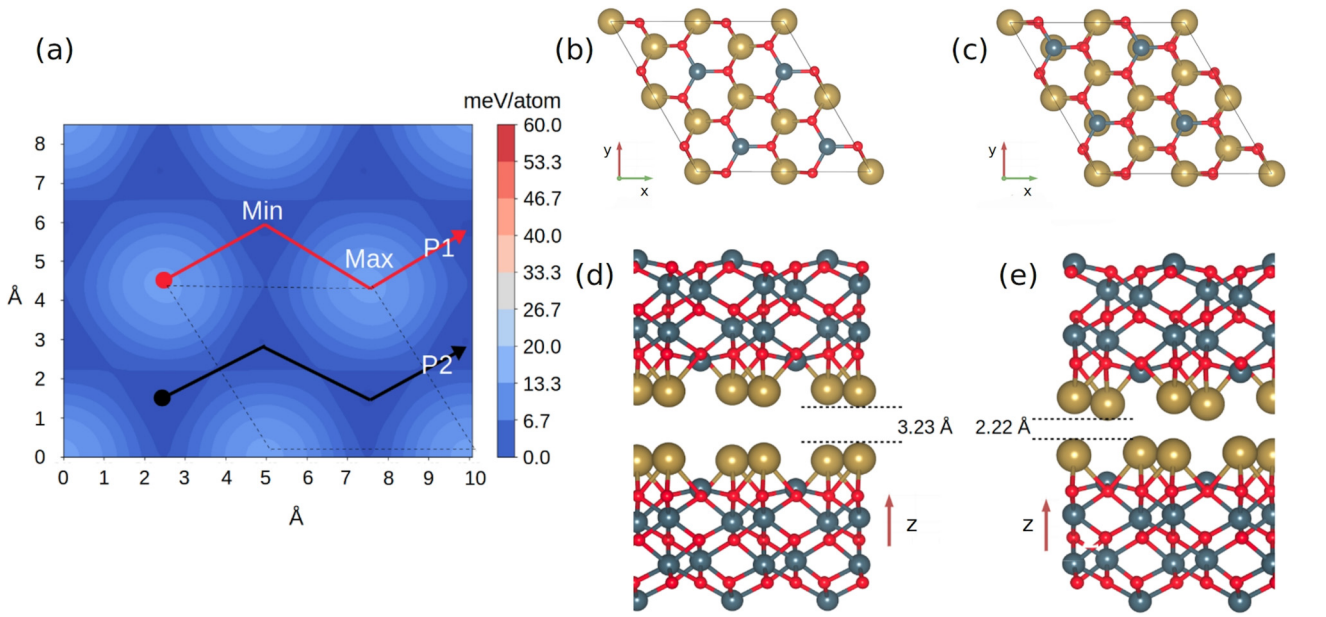

FIG. 7. PES as a function of relative displacement of the two passivated substrates (a), the black and red solid line mark the minimum and maximum energy pathways, the dashed line represents a unit cell. Geometric arrangement for the most important stacking configurations [maximum (c) and minimum (d)] in the PES of the Na-passivated surfaces, the bottom pictures (d) and (e) show the side view of the corresponding structures, respectively. Only the three topmost atomic layers of the lower slab and three bottom layers of the upper slab are shown in the top view images.

Isosurfaces of the charge density indicate that the interaction between two sodium passivated surfaces is smaller than that of iron oxide surfaces only. The peaks of the planar averaged charge density difference at the maximum and minimum energy configurations [Fig. 8(b)] of the sodium passivated system are, respectively, 1.3 and 4.7 times smaller than that of the pure iron oxide surface [Fig. 4(b)]. The quantitative values of the charge redistribution at the interface calculated using Eq. (4) are shown in Table I. The charge redistribution of the minimum configuration is significantly reduced from 40.0 to 14.6×10^{-4} e/Å^3 when the surfaces are covered by sodium atoms. Meanwhile, the maximum structure experiences a smaller decrease in the charge redistribution (from 22.9 to 20.0×10^{-4} e/Å^3). It is worth mentioning that the charge redistribution of the sodium passivated surfaces is strongly located outside the interface [Fig. 8(b)], especially at the maximum energy configuration. Therefore, the charge density difference at the interface remains at low values. The result suggests that less energy is needed to redistribute the charge when two sodium passivated surfaces slide against each other.

The explanation for the decline of charge density difference is straightforward. As mentioned in Sec. III B, the charge accumulation and depletion at the Fe_2O_3–Fe_2O_3 interface derives from the strong covalent interaction between Fe and O atoms of the two surfaces. The adsorption of sodium on the iron oxide surfaces, however, screens those direct interactions and prevents the charge transfers from the oxide layers in contact toward the interface. Such a hindrance of charge flow may reduce the adhesion as well as the friction of the oxide surface. Since the charge redistribution at the interface has a positive correlation with potential corruption as well as friction,[32] the manipulation of the charge redistribution using alkali passivation allows us to control the friction of the two sliding surfaces.

The evolution of the energies and averaged lateral forces with the displacement along the two sliding pathways (minimum and maximum energy pathways) is shown in Fig. 9 and Table I, respectively. A remarkable note is that the energy barriers for moving along the maximum and minimum energy pathways are significantly lower compared with those of pure oxide surfaces. Particularly, the maximum energy pathway peaks at 12.5 meV/atom while the minimum one only reaches 2.1 meV/atom (Fig. 9), which are, respectively, 3.7 and 10.7 times smaller than those of the nonpassivated surface. Another notable point is that the sodium passivated surface needs a longer sliding distance to reach its peaks when moving along the maximum (2.90 Å) and minimum (1.30 Å) energy pathways compared to that of nonpassivated surface (1.72 and 1.32 Å). The result is due to the change in the surface topology by the Na adsorption which, in turn, modifies the PES. In this study, the quantitative shear strength along a specific direction is derived by dividing the averaged lateral friction to the contact area,[64]

$$\tau = F/A, \tag{6}$$

where F is the averaged lateral friction and A is the surface area in the xy-plane. The average static lateral force is calculated by using the aforementioned method by Zhong and Tománek.[64] The smaller barrier energy and longer sliding distance of the passivated surface lead to a significant reduction of the shear strength along the chosen direction. The calculated shear strength for two different pathways is shown in Table I. In comparison with the clean iron oxide surface, sodium passivation helps to reduce the shear strength by 10 and 6 times along the minimum and maximum energy pathways, respectively. As mentioned in Sec. III B, the maximum amount of energy per atom that might be dissipated by frictional

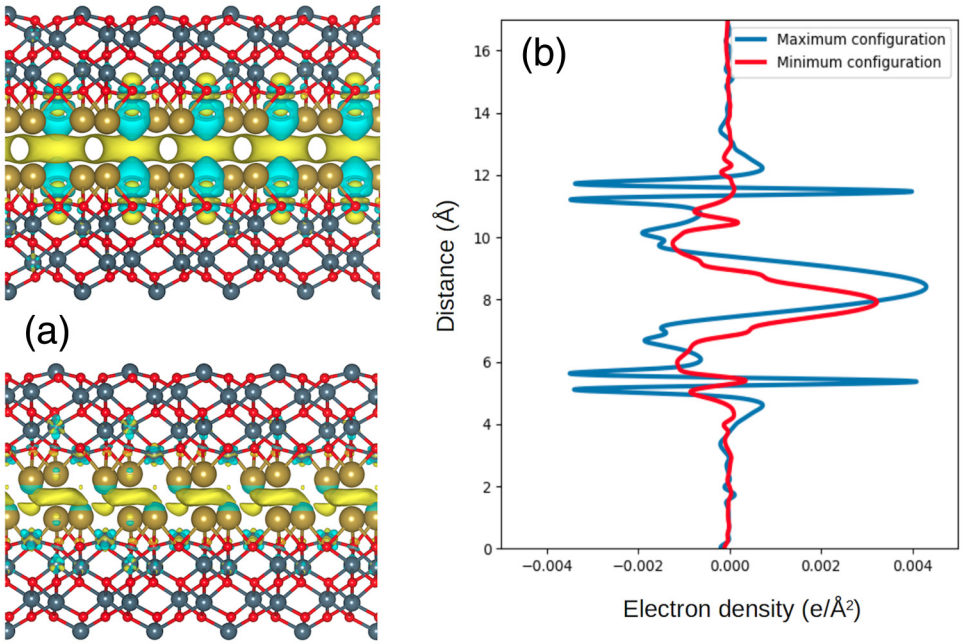

FIG. 8. (a) Charge density difference for the least (top) and the most (bottom) favorable stacking configurations of the two passivated surfaces in contact. The yellow and cyan represent the positive (electron accumulation) and negative (electron depletion) regions, respectively (isosurfaces are 0.001 e/Å^3). (b) Planar average of the electronic charge displacements occurring upon the stacking of two iron oxide surfaces. Blue and red colors are used for the charge displacements calculated respectively for the least and the most favorable lateral positions. It is noted that the isosurfaces value used in this figure is five times smaller than that of Fig. 4.

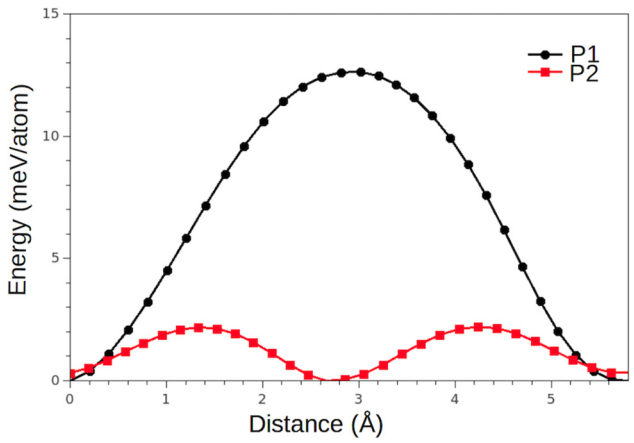

FIG. 9. Variation of the system energies with the sliding displacement along the maximum (black line) and minimum (red line) energy pathways marked in Fig. 7(a).

processes is the corrugation energy, which measures the energy difference between the minimum and the maximum of the PES. Our calculation indicates that the corrugation energy is lowered by approximately 3.7 times when the oxide surface is passivated by sodium (from 46.5 meV/atom to 12.5 meV/atom). The increasing interlayer distance as well as the lowering of the corrugation energy suggesting that the sodium element released by glass lubricants can reduce the adhesion between two surfaces in contact. A previous experimental study by Cui *et al.*[20] on three different types of sodium phosphates has shown that the compounds can greatly reduce the friction coefficient at high temperatures and pressures. More importantly, the study has proven that the compound with the highest concentration of sodium provides the lowest friction. According to their data, the friction coefficient can be reduced three times by using sodium orthophosphate Na_3PO_4. In addition, Tran *et al.*[19] also proved that sodium atoms in the borate glass play a crucial role in friction reduction. By comparing the lubrication performance of B_2O_2 and Na_2O-B_2O_3, they showed that the friction coefficient of the latter compound is five to six times lower than that of the former one. Furthermore, the wear can be reduced by nine times when the sodium element is added. Those results are consistent with the findings from our calculation. Although the tendency found in our simulation is similar to what has been found in the experimental studies, it is worth mentioning that glass lubricating systems are the complex ones. In addition, under the harsh working condition of high temperatures and pressures, the lubricant can be very chemically active and react with the oxide surface. As a result, other factors such as effects of pressure, temperature, shear, and the surface modifications due to chemical reactions with other elements of the lubricant should not be ruled out in tribological simulation models. The roles of those factors will be discussed in our future work.

D. Effects of load on tribological properties

To study the influence of pressure on the interfacial interaction and friction, the evolution of the corrugation energy as well as the charge redistribution under different loads, have been examined. Starting with the maximum and minimum configurations of the clean and passivated systems obtained in Secs. III B and III C, the freedom in the x, y, and z-directions of the three topmost layers being constrained when the relaxations are performed with several different separation distances. In all calculations, the upper slab is shifted by 0.1 Å every step along the z-direction. Finally, the data are made finer using the spline interpolation. The normal pressure, σ_N, is obtained by calculating the normal load, $F_\perp = -\partial E/\partial z$, then divided by the contact area of the interface A.

Figure 10(a) illustrates the evolution of the corrugation energy as well as the interlayer distance under the pressure from 0 to 5 GPa. An increasing load will result in a rise in the corrugation energy (from 46.5 to 47.9 meV/atom) for iron oxide surface. However, passivating the surface by sodium reduces the corrugation energy from 12.5 to 14.7 meV/atom for the same pressure range

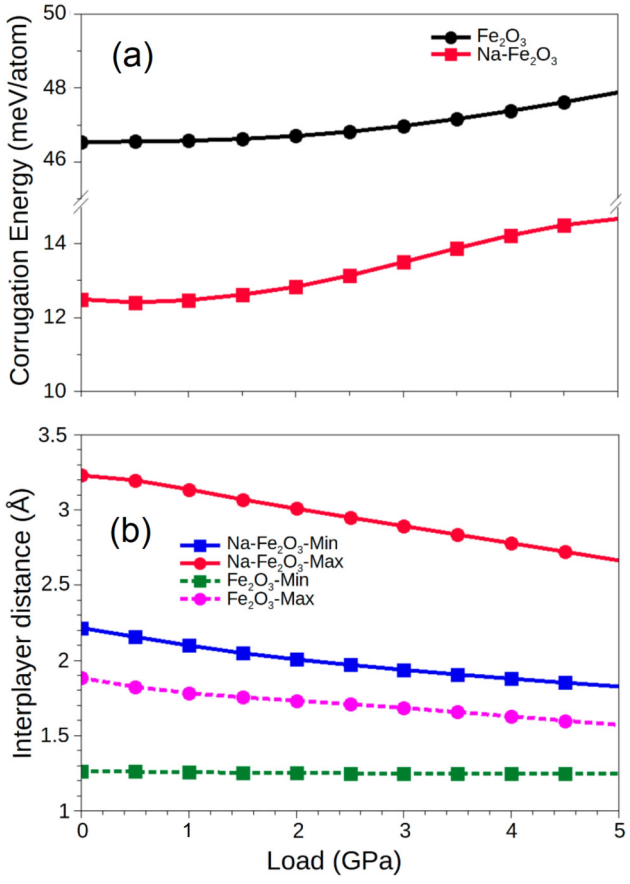

FIG. 10. (a) The variation of the system energy corrugation with load for clean (black line) and passivated (red line) systems. (b) The dependence of interlayer distance with load for the maximum and minimum configurations of the two systems. The solid and dash lines represent the pure iron oxide and sodium passivated surfaces, respectively. The circle symbol indicates the maximum configuration, while the square sign marks the minimum one.

(0–5 GPa). It is worth mentioning that the lower corrugation energy of the passivated surface compared to that of the clean one at high pressures demonstrates the high efficiency of the sodium tribofilm layer even under harsh working conditions.

The interlayer distance of the passivated system is more sensitive to pressure compared to that of the clean surface. This effect becomes clear when the system is at the lowest energy configuration. As shown in Fig. 10(b), the interlayer distance of the passivated system is reduced from 2.22 to 1.84 Å (0.38 Å) at the minimum configuration when the pressure increases from 1 to 5 GPa. Meanwhile, the nonpassivated oxide surface shows almost no change in the interlayer distance for the same pressure range. The reason is due to the electrostatic interaction between the sodium layers. This weak and long-range interaction allows the two sodium layers to flexibly alter their bond lengths compared to the covalent bonds in the case of the iron oxide surface. However, the interlayer distances of the Na-passivated systems are still much higher than those of the clean surfaces thanks to the repulsive force between two positive charged layers of sodium. Wang *et al.*[33] have found that the smaller interlayer distance may lead to a larger variation of the dispersion energy and vice versa. In addition, there is a positive correlation between the corrugation energy and the variation of the dispersion energy. As a consequence, the relatively small variation of dispersion energy due to the large interlayer distance in the sodium passivated surface may contribute to the low system corrugation energy and consequently a reduced friction at high pressures.

To gain further insight into the effects of pressure on the PES corrugations, we examine the behavior of charge density for the pressure-driven structures. Figure 11(a) shows that the pure Fe_2O_3 system exhibits a little change in the charge density difference when the pressure increases from 0 to 5 GPa, especially for the stable stacking configuration. Particularly, the integration of the planar averaged charge difference indicates that the charge at the interface increases slightly from 22.9 to 27.9×10^{-4} e/Å^3 for the maximum energy configuration. Meanwhile, there is almost no modification of the charge density at the minimum energy stacking (39.6×10^{-4} e/Å^3). This is due to the fact that the clean oxide surface only needs a small amount of displacement to reach the desired pressure (0.23 and 0.36 Å for the minimum and maximum energy configurations), which leads to a trivial change in the interlayer distance [Fig. 10(b)] as well as the charge density difference. As a consequence, the corrugation energy of the pure oxide surface shows only a slight increase when the pressure is raised to 5 GPa [Fig. 10(a)].

Interestingly, the charge density difference of passivated systems [Fig. 11(b)] also shows a minimal change at a high pressure (5 GPa), although the variation of the interlayer distance is more significant compared with that of the pure oxide surface. The integration of the planar averaged charge difference indicates that the charge at the interface only increases slightly from 14.6 and 20.0 to 15.1 and 21.7×10^{-4} e/Å^3 for the minimum and maximum energy configurations. Unlike the case of the pure oxide surface where the small modification of the charge redistribution is due to the minimal change in the interlayer distance, the larger interlayer variation of the passivated surface suggests that there should be a mechanism to minimize the charge redistribution. A remarkable point is that most of the charge redistribution of the Na-passivated surface is mainly located at the region right above or below the interface where the sodium layers interact with the iron oxide substrates (Figs. 8 and 11). We believe that this layer plays an important role as a pad that adsorbs the effect of load. Figure 11(b)

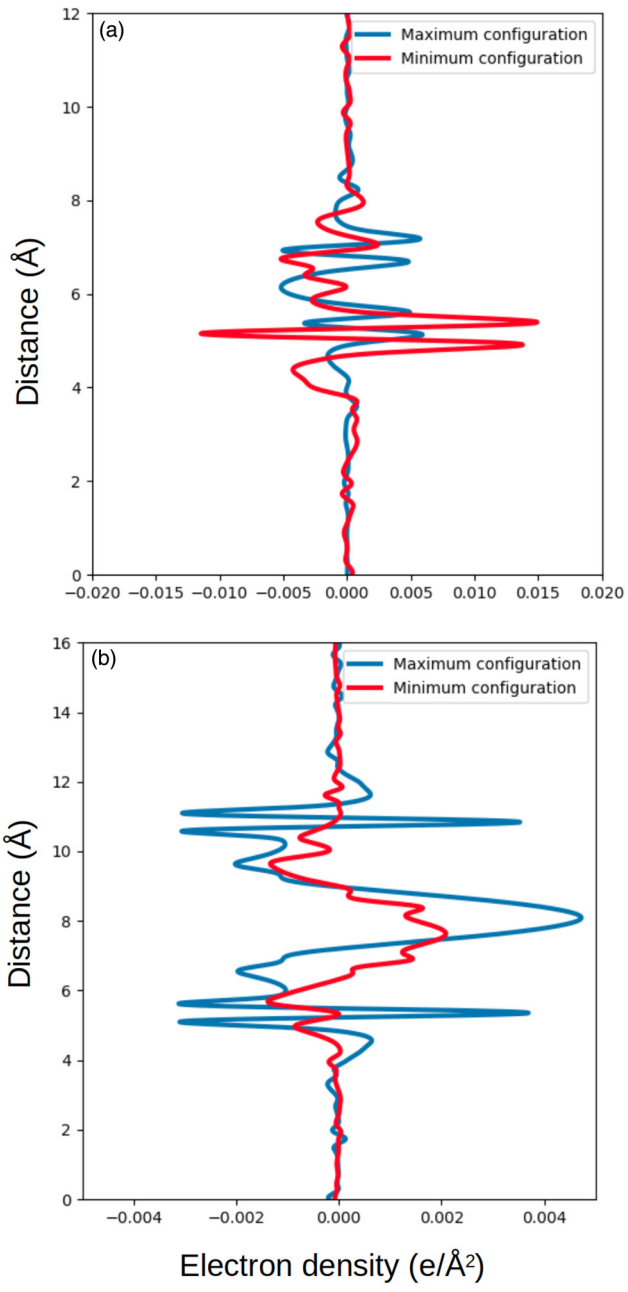

FIG. 11. Planar average of the electronic density difference for the stable and unstable stacking configurations of the clean (a) and the passivated surface (b) under a load of 5 GPa. Blue and red colors are used for the charge displacements calculated at the unstable and stable lateral positions respectively.

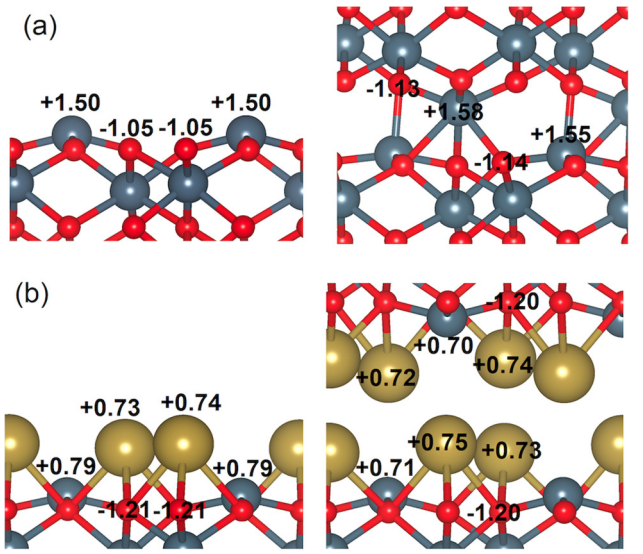

FIG. 12. Bader charge analysis of the pure (a) and passivated (b) iron oxide surface before (left) and after (right) the compression at 5 GPa.

shows that the main peak of the planar averaged charge difference of the minimum configuration is slightly shrunk and expanded into both sides of the interface. The result shows a tendency to disperse the charge redistribution to the padding layers. This mechanism might help the passivated surface to minimize the charge redistribution when the interlayer distance is strongly reduced.

To further quantify the charge transfer, the Bader analysis has been performed to estimate the point charge of each atom at the sliding interface, the results are displayed in Fig. 12 and Table II. The calculated charge of Fe atoms on the pure iron oxide surface is +1.50*e* [Fig. 12(a), left], which is significantly smaller than that of the bulk structure (∼+1.70*e*). This is due to the fact that Fe atoms on the surface have fewer bonds with the surrounding oxygen, therefore, they donate less electrons compared with the Fe atoms in the bulk. On the contrary, the oxygen atoms at the lower layer receive less electrons and have a point charge of −1.05*e* (compared to that of −1.08*e* in the bulk structure). When the two pure iron oxide surfaces are brought into contact at a high pressure (5 GPa), the Fe—O bond formation leads to a mutual charge transfer between the two layers [Fig. 12(a), right]. Generally, the Fe atoms at the interface donate their electrons to the oxygen atoms of the opposite layer causing their net charge to increase from +1.50*e* up to +1.58*e*. Meanwhile, the net charge of the oxygen atoms is reduced by 0.08–0.09*e* due to the donated electrons from Fe. This result indicates that a large amount of charge reconstruction has occurred at the interface of the system. When sodium atoms are adsorbed on the surface, they transfer their electrons to the lower atomic layers. As shown in Fig. 12(b) (left), the net charge of Fe and O atoms is reduced significantly from +1.50 and −1.05*e* to +0.79 and −1.21*e*, respectively. In contrast to the case of Fe atoms in the pure iron oxide surface, the Na atoms at the passivated interface show a smaller amount of charge variation as illustrated in Fig. 12(b) (right). However, there is a remarkable charge accumulation at the lower Fe atomic layer. Particularly, the charge of Fe atoms in this layer is reduced from +0.79*e* to a low value of +0.70*e*, while the O layer below slightly loses its electrons. As shown in Table II, the Fe atom at the interface of the pure surface loses 0.055*e* per atom on average when they are brought into contact at high pressures. Meanwhile, when the surface is passivated by Na, the charge of these interface atoms only varies by 0.001*e*. At the same time, the Fe layer below and above the sodium layer experienced a significant averaged charge accumulation of 0.082 e per atom. The result confirmed our explanation that sodium passivation will create a padding layer, which can reduce the charge reconstruction at the interface.

TABLE II. Bader charge transfer of Fe, O, and Na atoms at the interface after the two surfaces is brought into contact at a high pressure (5 GPa). A positive value means electron loss and vice versa. The unit is e/atom.

Systems	Fe-surface	O-surface	Na
Fe_2O_3	+0.055	−0.035	
Na-Fe_2O_3	−0.082	+0.014	−0.001

IV. CONCLUSIONS

DFT calculations have been performed to construct the potential energy surface (PES) of two iron oxide surfaces in contact as a function of the lateral sliding of the upper slab relative to the lower one. The shear strength, interfacial interactions, static lateral friction, and corrugation energy are quantitatively calculated and analyzed. The maximum and minimum energy pathways are also derived from the PES. In addition, the stability and friction of the sodium passivated Fe_2O_3 (0001) surfaces in different configurations are systematically studied and compared with those of the clean oxide surfaces. The key findings are summarized below:

(1) The high shear strength and lateral friction of iron oxide surface are caused by the formation of the Fe—O covalent bonds for some lateral arrangements. These bonds lead to a large corrugation of the PES as well as a small interlayer distance between the two layers. The calculated charge density difference shows that a large amount of charge is redistributed at the interface because of the formation of the Fe—O bonds between the two layers when the top layer slides from unstable to stable configurations. The result suggests that a huge amount of energy is needed to reconstruct the electron distribution.
(2) Sodium atoms have a tendency to adsorb on the hollow position of the Fe_2O_3 (0001) surface. The adsorption of sodium at a high coverage greatly reduces the shear strength and lateral friction of the passivated surfaces by significantly collapsing the PES. Due to the adsorbed Na layers, the formation of the Fe—O bonds between the two layers is eliminated and the interlayer distance of the two passivated surfaces is maintained at a high value. The charge density difference at the interface shows a minor change when the top layer moves from unstable to stable stacking.

(3) The interlayer distance between the two sodium passivated surfaces is more vulnerable to the external load than that of the pure surface, but it still remains at a high value. The passivation of sodium can create a padding layer on the oxide surface and reduce the effect of load by dispersing the charge redistribution to these padding layers. Therefore, the sliding of the passivated surfaces is expected to retain the low friction even at high pressures.

SUPPLEMENTARY MATERIAL

See the supplementary material for the absorption energy of sodium on the $Fe_2O_3(0001)$ surface at different locations and coverages, and the potential energy surface of the Na-passivated surface at different coverages.

ACKNOWLEDGMENTS

This project is supported by an Australian Research Council Discovery Project (No. DP 170103173) and Linkage (No. LP160101871). The authors would like to thank the National Computational Infrastructure (NCI) Australia for computing time on high-performance computing environment and Keith Brophy from UOW HPC for his support.

The authors declare no competing financial interest.

REFERENCES

[1]M. Salasi, T. Shahrabi, E. Roayaei, and M. Aliofkhazraei, Mater. Chem. Phys. **104**(1), 183–190 (2007).
[2]K. Matsumoto, M. Izawa, T. Nakanishi, and K. Tsubouchi, Tribol. Trans. **52**(4), 553–559 (2009).
[3]W. Yue, C. Wang, Y. Liu, H. Huang, Q. Wen, and J. Liu, Tribol. Trans. **53**(2), 288–295 (2010).
[4]Y. Yu, J. Gu, F. Kang, X. Kong, and W. Mo, Appl. Surf. Sci. **253**(18), 7549–7553 (2007).
[5]W. H. Zachariasen, J. Am. Chem. Soc. **54**(10), 3841–3851 (1932).
[6]B. E. Warren and J. Biscob, J. Am. Ceram. Soc. **21**(7), 259–265 (1938).
[7]B. E. Warren, Phys. Rev. **45**(10), 657–661 (1934).
[8]G. N. Greaves, A. Fontaine, P. Lagarde, D. Raoux, and S. J. Gurman, Nature **293**(5834), 611–616 (1981).
[9]H. W. Nesbitt, G. S. Henderson, G. M. Bancroft, and R. Ho, J. Non-Cryst. Solids **409**, 139–148 (2015).
[10]N. Zotov, J. Non-Cryst. Solids **287**(1), 231–236 (2001).
[11]J. O. Isard, J. Non-Cryst. Solids **1**(3), 235–261 (1969).
[12]L. Shartsis, S. Spinner, and W. Capps, J. Am. Ceram. Soc. **35**(6), 155–160 (1952).
[13]J. O. M. Bockris, J. D. Mackenzie, and J. A. Kitchener, Trans. Faraday Soc. **51**(0), 1734–1748 (1955).
[14]C. A. Faick and A. N. Finn, J. Am. Ceram. Soc. **14**(7), 518–528 (1931).
[15]T. Uchino, M. Iwasaki, T. Sakka, and Y. Ogata, J. Phys. Chem. **95**(14), 5455–5462 (1991).
[16]H. T. T. Ta, A. K. Tieu, H. Zhu, H. Yu, T. D. Ta, S. Wan, N. V. Tran, and H. M. Le, J. Phys. Chem. C **122**(1), 635–647 (2018).
[17]S. Wan, A. K. Tieu, Q. Zhu, H. Zhu, S. Cui, D. R. G. Mitchell, C. Kong, B. Cowie, J. A. Denman, and R. Liu, Sci. Rep. **6**, 26008 (2016).
[18]B. H. Tran, A. K. Tieu, S. Wan, H. Zhu, D. R. G. Mitchell, and M. J. Nancarrow, J. Phys. Chem. C **121**(45), 25092–25103 (2017).
[19]B. H. Tran, K. Tieu, S. Wan, H. Zhu, S. Cui, and L. Wang, RSC Adv. **8**(51), 28847–28860 (2018).
[20]S. Cui, S. Wan, Q. Zhu, A. K. Tieu, H. Zhu, L. Wang, and B. Cowie, J. Phys. Chem. C **120**(45), 25742–25751 (2016).
[21]L. Wang, A. K. Tieu, H. Zhu, S. Cui, G. Deng, G. Hai, and J. Yang, J. Phys. Chem. C **123**(23), 14468–14479 (2019).
[22]Y. Feng, N. Wang, and X. Guo, Fuel **236**, 1057–1064 (2019).
[23]S. Kolev, P. S. Petkov, M. Rangelov, and G. N. Vayssilov, ACS Chem. Biol. **8**(7), 1576–1589 (2013).
[24]S. Kajita and M. C. Righi, Carbon **103**, 193–199 (2016).
[25]P. Restuccia and M. C. Righi, Carbon **106**, 118–124 (2016).
[26]G. Zilibotti, S. Corni, and M. C. Righi, Phys. Rev. Lett. **111**(14), 146101 (2013).
[27]S. Zhang, T. Ma, A. Erdemir, and Q. Li, Mater. Today **26**, 67–86 (2019).
[28]J. Sun, Y. Zhang, Z. Lu, Q. Li, Q. Xue, S. Du, J. Pu, and L. Wang, J. Phys. Chem. Lett. **9**(10), 2554–2559 (2018).
[29]N. V. Tran, A. K. Tieu, H. Zhu, H. T. T. Ta, T. D. Ta, and H. M. Le, J. Phys. Chem. C **122**(36), 20827–20840 (2018).
[30]M. H. Le, A. K. Tieu, H. Zhu, D. T. Ta, H. Yu, T. T. H. Ta, V. N. Tran, and S. Wan, Phys. Chem. Chem. Phys. **20**(11), 7819–7835 (2018).
[31]V. Jaiswal, R. B. Rastogi, J. L. Maurya, P. Singh, and A. K. Tewari, RSC Adv. **4**(26), 13438–13445 (2014).
[32]M. Wolloch, G. Levita, P. Restuccia, and M. C. Righi, Phys. Rev. Lett. **121**(2), 026804 (2018).
[33]L. F. Wang, T. B. Ma, Y. Z. Hu, H. Wang, and T. M. Shao, J. Phys. Chem. C **117**(24), 12520–12525 (2013).
[34]G. Ketteler, W. Weiss, W. Ranke, and R. Schlögl, Phys. Chem. Chem. Phys. **3**(6), 1114–1122 (2001).
[35]P. Giannozzi, S. Baroni, N. Bonini, M. Calandra, R. Car, C. Cavazzoni, D. Ceresoli, G. L. Chiarotti, M. Cococcioni, I. Dabo, A. Dal Corso, S. de Gironcoli, S. Fabris, G. Fratesi, R. Gebauer, U. Gerstmann, C. Gougoussis, A. Kokalj, M. Lazzeri, L. Martin-Samos, N. Marzari, F. Mauri, R. Mazzarello, S. Paolini, A. Pasquarello, L. Paulatto, C. Sbraccia, S. Scandolo, G. Sclauzero, A. P. Seitsonen, A. Smogunov, P. Umari, and R. M. Wentzcovitch, J. Phys. Condens. Matter **21**(39), 395502 (2009).
[36]P. Giannozzi, O. Andreussi, T. Brumme, O. Bunau, M. Buongiorno Nardelli, M. Calandra, R. Car, C. Cavazzoni, D. Ceresoli, M. Cococcioni, N. Colonna, I. Carnimeo, A. Dal Corso, S. de Gironcoli, P. Delugas, R. A. DiStasio, A. Ferretti, A. Floris, G. Fratesi, G. Fugallo, R. Gebauer, U. Gerstmann, F. Giustino, T. Gorni, J. Jia, M. Kawamura, H. Y. Ko, A. Kokalj, E. Küçükbenli, M. Lazzeri, M. Marsili, N. Marzari, F. Mauri, N. L. Nguyen, H. V. Nguyen, A. Otero-de-la-Roza, L. Paulatto, S. Poncé, D. Rocca, R. Sabatini, B. Santra, M. Schlipf, A. P. Seitsonen, A. Smogunov, I. Timrov, T. Thonhauser, P. Umari, N. Vast, X. Wu, and S. Baroni, J. Phys. Condens. Matter **29**(46), 465901 (2017).
[37]J. P. Perdew, K. Burke, and M. Ernzerhof, Phys. Rev. Lett. **77**(18), 3865–3868 (1996).
[38]J. P. Perdew, J. A. Chevary, S. H. Vosko, K. A. Jackson, M. R. Pederson, D. J. Singh, and C. Fiolhais, Phys. Rev. B **46**(11), 6671–6687 (1992).
[39]D. Vanderbilt, Phys. Rev. B **41**(11), 7892–7895 (1990).
[40]H. J. Monkhorst and J. D. Pack, Phys. Rev. B **13**(12), 5188–5192 (1976).
[41]A. Patra, J. E. Bates, J. Sun, and J. P. Perdew, Proc. Natl. Acad. Sci. U.S.A. **114**(44), E9188 (2017).
[42]H. Peng and J. P. Perdew, Phys. Rev. B **96**(10), 100101 (2017).
[43]J. Yu, J. Zhang, and S. Liu, J. Phys. Chem. C **114**(32), 13642–13649 (2010).
[44]S. Grimme, J. Comput. Chem. **27**(15), 1787–1799 (2006).
[45]S. A. Chambers and S. I. Yi, Surf. Sci. **439**(1), L785–L791 (1999).
[46]J.-J. Tang and B. Liu, J. Phys. Chem. C **120**(12), 6642–6650 (2016).
[47]X. Huang, S. K. Ramadugu, and S. E. Mason, J. Phys. Chem. C **120**(9), 4919–4930 (2016).
[48]M. Wolloch, G. Feldbauer, P. Mohn, J. Redinger, and A. Vernes, Phys. Rev. B **90**(19), 195418 (2014).
[49]L. F. Wang, T. B. Ma, Y. Z. Hu, and H. Wang, Phys. Rev. B **86**(12), 125436 (2012).
[50]T. Liang, W. G. Sawyer, S. S. Perry, S. B. Sinnott, and S. R. Phillpot, Phys. Rev. B **77**(10), 104105 (2008).

[51]I. G. Batyrev, A. Alavi, and M. W. Finnis, Phys. Rev. B **62**(7), 4698–4706 (2000).
[52]T. Yang, X. D. Wen, Y. W. Li, J. Wang, and H. Jiao, Surf. Sci. **603**(1), 78–83 (2009).
[53]C. Mazzara, J. Jupille, A. M. Flank, and P. Lagarde, J. Phys. Chem. B **104**(15), 3438–3445 (2000).
[54]D. L. Price, Curr. Opin. Solid State Mater. Sci. **1**(4), 572–577 (1996).
[55]A. Kiejna and T. Pabisiak, J. Phys. Condens. Matter **24**(9), 095003 (2012).
[56]A. Groysman, *Corrosion for Everybody* (Springer, Netherlands, 2010).
[57]S. Musić, S. Krehula, and S. Popović, Mater. Lett. **58**(3), 444–448 (2004).
[58]D. Cao, H. Li, L. Pan, J. Li, X. Wang, P. Jing, X. Cheng, W. Wang, J. Wang, and Q. Liu, Sci. Rep. **6**, 32360 (2016).
[59]N. S. Petro and B. S. Girgis, J. Therm. Anal. **34**(1), 37–45 (1988).
[60]Z. Łodziana, J. K. Nørskov, and P. Stoltze, J. Chem. Phys. **118**(24), 11179–11188 (2003).
[61]L. Wang, X. Zhou, T. Ma, D. Liu, L. Gao, X. Li, J. Zhang, Y. Hu, H. Wang, Y. Dai, and J. Luo, Nanoscale **9**(30), 10846–10853 (2017).
[62]S. Cahangirov, S. Ciraci, and V. O. Özçelik, Phys. Rev. B **87**(20), 205428 (2013).
[63]M. Reguzzoni, A. Fasolino, E. Molinari, and M. C. Righi, Phys. Rev. B **86**(24), 245434 (2012).
[64]W. Zhong and D. Tománek, Phys. Rev. Lett. **64**(25), 3054–3057 (1990).
[65]M. I. De Barros-Bouchet, M. C. Righi, D. Philippon, S. Mambingo-Doumbe, T. Le-Mogne, J. M. Martin, and A. Bouffet, RSC Adv. **5**(61), 49270–49279 (2015).
[66]J. Krim, Adv. Phys. **61**(3), 155–323 (2012).
[67]J. Y. Park and M. Salmeron, Chem. Rev. **114**(1), 677–711 (2014).
[68]M. Cieplak, E. D. Smith, and M. O. Robbins, Science **265**(5176), 1209 (1994).
[69]M. Pierno, L. Bruschi, G. Fois, G. Mistura, C. Boragno, F. B. de Mongeot, and U. Valbusa, Phys. Rev. Lett. **105**(1), 016102 (2010).